applied optics

Diffraction model for thermoreflectance data

S. Kureshi,* D. Fabris, S. Tokairin, C. V. Cardenas, and C. Y. Yang

Center for Nanostructures, Santa Clara University, Santa Clara, California 95053, USA
*Corresponding author: skureshi@scu.edu

Received 20 August 2014; revised 25 March 2015; accepted 5 May 2015; posted 6 May 2015 (Doc. ID 220919); published 4 June 2015

Thermoreflectance imaging provides the capability to map temperature spatially on the submicrometer scale by using a light source and CCD camera for data acquisition. The ability to achieve such spatial resolution and observe detailed features is influenced by optical diffraction. By combining diffraction from both the sample and substrate, a model is developed to determine the intensity of the thermoreflectance signal. This model takes into account the effective optical distance, sample width, wavelength, signal phase shift, and reflectance intensity, while showing qualitative and quantitative agreement with experimental thermoreflectance images from 1 and 10 μm wide gold lines at two wavelengths. © 2015 Optical Society of America

OCIS codes: (050.1940) Diffraction; (110.6820) Thermal imaging; (120.6780) Temperature.

http://dx.doi.org/10.1364/AO.54.005314

1. INTRODUCTION

The size of nanoelectronic devices is continuously shrinking to achieve higher speed of operation and lower fabrication cost for given performance. Recently, the minimum feature size in integrated circuits (ICs) has decreased to smaller than 24 nm [1]. For reliable operation of these nanoscale devices, it is necessary to study the temperature in the submicrometer scale [2,3]. Temperature measurement is divided in two main categories: contact and noncontact methods. Noncontact methods offer some advantages over contact thermal measurements. For example, there is no sensor loading bias, risk of contamination, or mechanical effects on the surface. With thermoreflectance, it is possible to measure the full-field temperature at high speeds [4,5]. However, full-field noncontact methods are spatially limited by diffraction, which is based on the wavelength of light used during measurement. Different methods for temperature measurement on micro- and nanoscale electronic and photonic devices are summarized by Christofferson *et al.* [5].

Thermoreflectance (TR) temperature measurement belongs to the class of noncontact temperature measurements and uses an LED or filtered white light source and a CCD to acquire images. Thermoreflectance temperature measurement is based on the principle that a change in temperature of a given material produces a small change in the spectral reflectivity of the material's surface [4–7]. This small change can be linearized over a range of temperature. The linearized response of the normal reflectance with respect to the temperature of a sample allows the following approximation for the derivative of normal reflectance [8]:

$$\frac{\partial \rho_n}{\partial T} \approx \frac{\rho_n(T) - \rho_n(T_0)}{T - T_0}. \tag{1}$$

The normal reflectance intensity at a given temperature $I_n(T)$ can be calculated from

$$I_n(T) = \rho_n(T) \cdot I_0, \tag{2}$$

where $\rho_n(T)$ is normal reflectance and I_0 is incoming illumination intensity.

The spectral TR coefficient κ is defined by the normalization of the slope as a function of temperature with the reference quantity [8]

$$\kappa = \frac{1}{\rho_n(T_0)} \frac{\partial \rho_n}{\partial T} = \frac{1}{I_n(T_0)} \frac{\partial I_n}{\partial T}. \tag{3}$$

The thermoreflectance coefficient is a material and surface property that depends on the illumination wavelength, temperature, material surface characteristics, and in some cases also on the material processing [8]. For most metals and semiconductor materials of interest, the value of the thermoreflectance coefficient will be on the order of $10^{-4}\,°C^{-1}$ to $10^{-5}\,°C^{-1}$ [8]. During the experiment, it is necessary to calibrate the system and obtain the thermoreflectance coefficient for the specific sample. Following the calibration, one can determine the temperature difference developed during heating through rearrangement of the governing relationship with a measurement of the relative reflectance:

$$\Delta T = (T - T_0) = \frac{1}{\kappa}\left(\frac{I_n(T) - I_n(T_0)}{I_n(T_0)}\right). \tag{4}$$

In addition to the temperature, reflectance intensity may show dependence on a number of parameters, like the spectral width of the illumination and spectral sensitivity of reflectance detection.

Spatial resolution for thermoreflectance is limited by diffraction [9]. Diffraction is defined as deviation of light rays from rectilinear that cannot be interpreted as reflection or refraction [10–13]. In the prior work, thermoreflectance was used to measure the temperature of thin gold films that modeled electrical interconnects. The modeled interconnects were 1–10 μm in width and tens of μm long. In this paper, a mathematical model is developed for better analysis of the thermoreflectance experimental data. The main purpose of this article is to understand the impact of diffraction and the parameters that govern the signal. A one-dimensional Fresnel diffraction formula is used to estimate diffracted field from the observed sample and the background. The mathematical model further takes into account the incoherent nature of the illumination source by averaging over the wavelengths of the light source. The remaining unknown parameters of the experiments are treated as free parameters and are determined by a comparison to the experimental data. A detailed explanation about diffraction theory and the mathematical model are discussed in Section 2.

Experimental data used here for comparison are taken from the Master's thesis of Cardenas [8] and briefly summarized in Section 3. The thermoreflectance technique was used to measure temperature and determine thermal contact resistance for gold thin film structures used as model electrical interconnects [7,8]. The observed sample consists of the gold thin film interconnects as seen in Fig. 1. The test interconnect consists of two gold pads, thin film leads, and a narrow test line connecting the two leads [14,15]. The gold film is deposited on an amorphous SiO_2 substrate grown on a silicon wafer. There is a thin adhesion layer of titanium between gold and SiO_2. This technique was extended to analyzing thermoreflectance data from 150 nm wide carbon nanofibers undergoing current stressing [16].

The thermoreflectance experiment was performed in two stages. In the calibration stage, the entire sample was uniformly heated to obtain the TR coefficient and the normal reflectance intensity was measured using a microscope and CCD. In the temperature measurement stage, the TR coefficient was then used to measure temperature distribution of the thin gold structure undergoing Joule heating. In prior experiments, the calibrated TR coefficient shows good agreement with the experimental work of Beran [17]. However, the calibrated TR coefficients under the illumination wavelengths of 470 and 530 nm yielded different values [8]. Whereas a temperature measurement from Joule heating was possible at 530 nm, the 470 nm data for the small interconnect lines were strongly influenced by diffraction. In both cases, but more pronounced at 470 nm, the size of the measurement sample affects the quality of the result. The combined effects of vibration and diffraction cause spatial averaging and convolution (blurring), and lead to mixing of the reflectance intensity of the gold film and substrate. The amount of diffraction depends upon the wavelength, the size of the sample, and the interaction with background. When measuring on the gold pads (10 μm wide), the thermal profiles obtained from the experiment for the wavelengths 470 and 530 nm match. The disagreement in the calibration and the measurement signal that exists over the narrow interconnect (1 μm wide) samples motivates the development of a diffraction-based model. We are not aware of any previous work that has investigated methods to use thermoreflectance on very narrow lines where diffraction has taken place. Grauby *et al.* discussed this problem but suggested no solution for thermoreflectance measurement [18]. The present work develops a model to characterize the diffraction based on the size of the sample, wavelength of the illumination, phase shift of the signal from the background, strength of the reflectance, and the apparent distance of the image. From fitting the model with the experimental data, the unknown parameters of the experiments are quantified. The parameters are the optical distance between the specimen and the CCD, and the phase shift between the signals resulting from the difference in the thickness of the gold line and the substrate. Results are discussed in detail in Section 4.

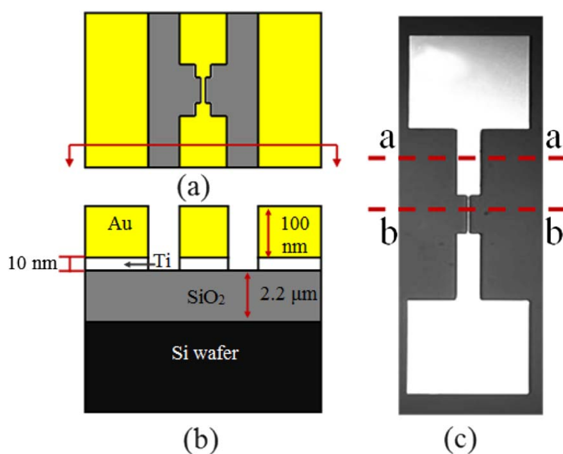

Fig. 1. Gold line sample used for electrical interconnect testing and thermoreflectance testing in prior work [7,14]. (a) Top view of sample; (b) section-view of sample; (c) microscopy-obtained reflectance intensity image under LED wavelength of 535 nm. Section a-a captures a region of the gold line structure at 10 μm wide, whereas in Section b-b the width is 1 μm.

2. MATHEMATICAL MODEL

The total reflected intensity imaged by the CCD is coming from two different surfaces with different reflectivity, the gold film and substrate. Accordingly, the mathematical model consists of two parts (Fig. 2): the reflectance intensity coming from the metallic gold film and the reflectance intensity coming from the background substrate. The two intensities are combined to yield the total reflected intensity. Light coming from the gold film is treated as diffraction through a slit due to the high reflectivity of gold. In the latter case, the reflected light coming from the substrate is obstructed by gold thin film on its way to the microscope. Hence, the reflection coming from the substrate is treated as diffraction past a strip.

We begin with the one-dimensional Fresnel formula of diffraction [19]:

$$E(x,z) = \sqrt{\frac{jk}{2\pi z}} e^{-jkz} \int_{-\infty}^{\infty} E(x_0,0) \exp\left(\frac{-jk(x-x_0)^2}{2z}\right) dx_0, \tag{5}$$

where E is the electric field density at distance z, and k is the wave number.

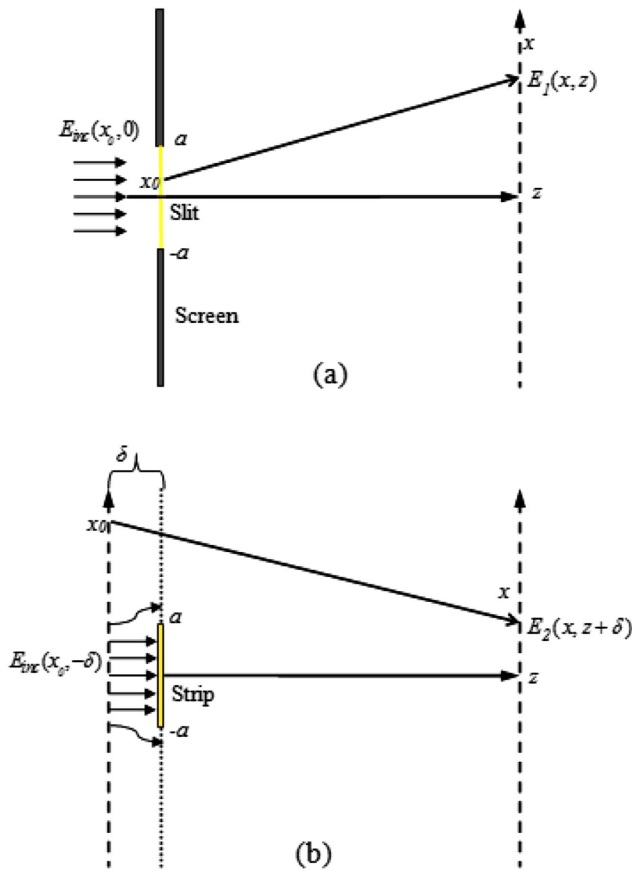

Fig. 2. Mathematical model setup composed of reflection from the sample and substrate based on two simple diffraction models. (a) Diffracted field for the gold line, where gold line is treated as slit. (b) Diffracted field for the substrate, where gold line is treated as a strip blocking the light reflected from the substrate.

The source is assumed to be a uniform incident field plane wave

$$E_{\text{inc}}(x,z) = E_0 e^{-jkz},$$

whose value at the slit is constant at

$$E_{\text{inc}}(x_0,0) = E_0.$$

The slit is considered of infinite dimensions in the y direction and, in the x direction, width is $2a$ as shown in Fig. 2(a). Then the diffracted field for the slit from Eq. (5) is given by

$$E_1(x,z) = \sqrt{\frac{jk}{2\pi z}} e^{-jkz} \int_{-a}^{a} \exp\left(\frac{-jk(x-x_0)^2}{2z}\right) \mathrm{d}x_0. \quad (6)$$

The integral can be reformulated into a Fresnel integral with the following change of variables [19]:

$$\sqrt{\frac{k}{2z}}(x_0 - x) = \sqrt{\frac{\pi}{2}} u \quad \& \quad v_{\pm} = \sqrt{\frac{k}{\pi z}}(\pm a - x). \quad (7)$$

With the substitutions of Eq. (7) into Eq. (6), one obtains

$$E_1(x,z) = \exp(-jkz)\left[\frac{\mathbb{F}(v_+) - \mathbb{F}(v_-)}{1-j}\right], \quad (8)$$

where, $\mathbb{F}(v)$ is the Fresnel integral.

The reflection coming from the substrate is treated as the diffraction past a strip of the same dimensions as the slit shown in Fig. 2(b). However the signal coming from the substrate is travelling a longer distance $2 \cdot \delta$ as compared to the signal originating from the gold line, which results in a phase shift between the two signals. The longer distance traveled accounts for the transparent silicon dioxide layer between the gold film and the reflective silicon substrate.

In the case of the strip

$$E_2(x, z+2\delta) = \exp(-j(kz-\varphi)) \times \left[\frac{\mathbb{F}(\infty) - \mathbb{F}(v_+) + \mathbb{F}(v_-) - \mathbb{F}(-\infty)}{1-j}\right], \quad (9)$$

and the total diffracted field can be obtained as

$$E_{\text{total}} = E_1 + \Gamma \cdot E_2, \quad (10)$$

where Γ is the ratio of the reflectivity of gold and the substrate material.

Then the total reflected intensity

$$I_{\text{total}} = E_{\text{total}} \cdot E^*_{\text{total}}. \quad (11)$$

In the experiment, the intensity measured by CCD is in arbitrary units. The model quantified total intensity in physical units. To compare the model with the experimental data, the total reflected intensity obtained from model is multiplied by the gain factor γ:

$$I_{\text{model}} = \gamma I_{\text{total}}. \quad (12)$$

3. EXPERIMENTAL SETUP

The experimental setup to perform normal reflectance intensity analysis as a function of sample temperature is shown in Fig. 3. It consists of an LED illumination source, CCD, optical microscope, sample holder, and acquisition equipment. A modified Meiji Techno microscope Series MC-50T is used as the central component of the system. A beam splitter is placed at the core of the microscope to guide collimated incident rays, and an aperture constrains the illumination beam onto the surface of the samples. Reflected light is transferred through the beam

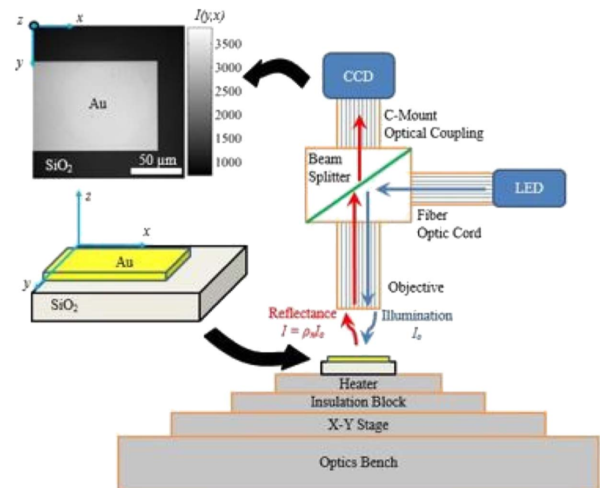

Fig. 3. Schematic of thermoreflectance temperature measurement experimental setup.

splitter to the CCD. A 12-bit A/D Prosilica GE1380 CCD camera is used to capture the reflectance intensity images. Illumination is generated from Luxeon Star/O series LEDs. The spectral characteristics of the two LEDs used in this research, as mentioned by manufacturer, are listed in Table 1. A custom-designed heater microscopy stage assembly is used to support samples while providing thermal control over a temperature range from ambient 20°C to 250°C [8].

The TR calibration coefficient κ is acquired prior to performing the measurements. Calibrations were performed for the two LEDs of central wavelengths 470 and 535 nm. Measurements of the sample temperature, T, and the normal reflectance intensity $I_n(T)$ over sufficiently large regions of the material were used to compute κ. Under LED illumination with a peak wavelength of 535 nm, the average value of the calibration coefficient was -1.71×10^{-4} °C^{-1} with a standard deviation of 0.19×10^{-4} °C^{-1}. Under LED illumination with 470 nm, the average value of the calibration coefficient was 1.76×10^{-4} °C^{-1} with a standard deviation of 2.1×10^{-5} °C^{-1}. These values demonstrate good agreement with the previous results of Beran for gold [17].

The second mode of the experiment is to acquire two-dimensional TR images of the calibrated structure during Joule heating. During this mode of operation, a function generator, amplification circuitry, and a delay generator are used to create a delay-locked loop tuned to acquire images of the periodically heated sample during the quasi-steady heating and relaxation regimes. A reflectance intensity image of the sample acquired under illumination at $\lambda_{\text{peak}} = 530$ nm is shown in Fig. 1(c). Following the acquisition of the heated and relaxed state images, processing was done for the computation of the temperature difference using TR coefficient and Eqs. (2) and (3). During Joule heating experiments, adequate manual correction of positioning with superposition of a reference image and a focal metric calculation are performed to correct for displacements due to the thermal expansion. The thermal expansion of the system is estimated to be 0.3% and does not result in a significant change in system size relative to the wavelengths considered. Due to high optical absorption of gold in the visible range, it was assumed during the experiment that the surface reflection is dominant and the film is sufficiently thick to be considered optically opaque. At 100 nm, the film thickness is 4.6 times the material's absorption coefficient, which governs the exponential decay of the electromagnetic wave in the gold. TR response has been shown to be linear over the calibration temperature range of 20°C–200°C.

4. RESULTS

The two-dimensional Joule-heating data for the sample were taken using the experimental setup for the wavelengths of 470 and 530 nm. For a single wavelength, the results are repeatable for increasing and decreasing current; however, for the same sample, the temperature distribution under two different LED wavelengths resulted in inconsistency.

Table 1. Spectral Characteristics of LEDs

Color	λ_{min} (nm)	λ_{peak} (nm)	λ_{max} (nm)	Spectral half-width $\Delta\lambda_{1/2}$ (nm)
Blue	460	470	490	25
Green	520	530	550	35

In our calculations, the following two unknowns in the experiment are considered as fitting parameters: optical distance z, the distance between the observed specimen and the imaged plane; and phase shift φ, the shift in phase between the signal coming from the gold line and the substrate. The optical distance is dependent on the overall imaging of the microscope and is treated as a fitting parameter. The phase shift is dependent on the thickness of the silicon dioxide layer, which is an increase in path length for the light to travel before reflecting off the silicon substrate. While treated as a fitting parameter, the phase shift must fall within a range consistent with this added path length. The effect of different z values is shown on each of the two components, in Fig. 4(a) for the slit $a = 4\lambda$ and Fig. 4(b) for the same size strip. As can be seen from these figures, the effect of diffraction is profound in the near field when $z = a$, whereas it is more blurred for the far field when $z = 50a$. The Fresnel number ($F = a^2/\lambda z$) in our cases spans the range from 0.1 to 3.5, which is on the order of 1. The Fraunhofer approximation is the limiting case when the optical distance z is large and $F \ll 1$. The Fresnel approximation is a partial series solution that is accurate in the limit $F \gg 1$, but can also be applied in the range $F \sim 1$ with lower accuracy due to the truncated terms in the series [13,19]. For a consistent approach, we have used the Fresnel calculation. The optical distance z is an unknown in the experiment and is used as a fitting parameter when the model is compared to the data.

The other two fitting parameters, reflectance ratio Γ and gain parameter γ, are for normalizing the overall intensity in the model with experimental data. The total reflectance intensity comes from two different surfaces, gold line and substrate, with different reflectivity. Further, to consider the optical absorption and the intensity of light source, the two diffracted field intensities are combined in the model with the help of the reflectance ratio Γ. The values of the material's reflectivity at

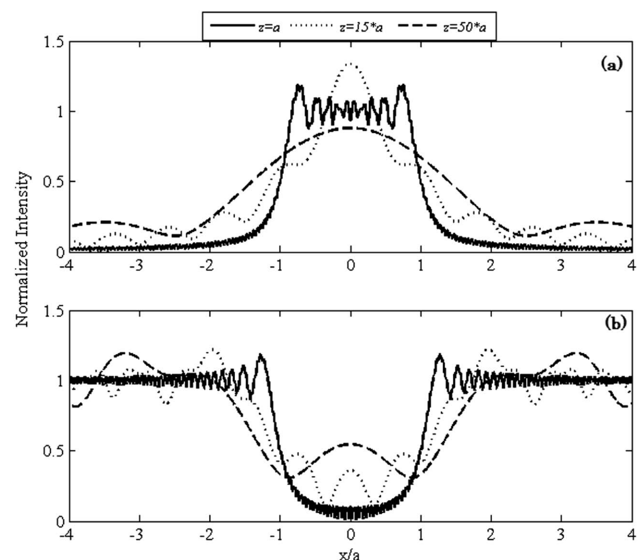

Fig. 4. Effect of distance z on diffracted field intensity for (a) slit and (b) strip for different image plane distances from the sample.

ambient temperature of 25°C depend upon the wavelength and are available in the literature [20]. The last fitting parameter is γ, a gain parameter that converts the normalized intensity signal to the range on the CCD.

To fit the model parameters with experimental data, least squares minimization is used to determine the best values for z and φ, starting from initial estimates of their values. This procedure is implemented in MATLAB. Since the experimental data are given in terms of averages of images from a CCD camera, the least squares procedure also normalizes the absolute image strength with a gain parameter and accounts for the difference in reflectivity of the gold and the silicon substrate, which is consistent with published reflectivity for the two materials.

During the experiment, the combined effects of vibration and noise smooth out the data and result in an intensity profile that lacks small-scale intensity signal variation seen in the model. This real filtering is due to the integration over the CCD pixels, physical vibration in the system, and diffraction in the optics. Therefore, some additional spatial average is applied to the model data. The spatial average is performed by calculating moving average over a window of 11 pixels, where each pixel is 0.0539 μm in width. As the LEDs used in the experiment are not monochromatic, the diffracted field and hence the reflectance intensity calculated with the mathematical model is integrated over the spectral width and strength of the LEDs. An attempt was made to take into account the incoherent nature of LEDs by performing phase average. Accounting for this wavelength variation did not significantly change the nature of the intensity profile.

In Fig. 5(a), the model is compared with the experimental data at the wide section for wavelength of 535 nm. The parameters used to generate these figures are summarized in Table 1. Although not an exact match, the model shows very good qualitative agreement with the experimental data. At the edge of the gold line, the model both underestimates and overestimates the intensity. This is caused mainly by the edge diffraction effect and limited experimental data available for the substrate signal. This small-scale oscillatory behavior is smoothed in the experimental data because of averaging in the CCD, vibration in the system, variation in the coherence of the light, and diffraction due to thermal gradient in the air above the sample.

In Fig. 5(b), the model data are compared with the experimental data at the same wide section but for a different illumination wavelength, 470 nm. Similar matching of the model and the experiment is observed. As the wavelength of illumination changes the reflectance, optical distance and phase shift should change. The new values of these parameters for the fitting are obtained from the algorithm confirmed in the theoretical values. The values are summarized in Table 2.

Figure 6(a) shows the fit for the narrow field at the wavelength of 530 nm. When moving from wide to narrow section for the same wavelength, the optical distance should change and as a result, the phase shifts. The values of these two parameters are varied to fit the model data to the experimental data. As can be seen, the model data fits with the experimental data except at the edge; again the model overestimates the experiment peaks.

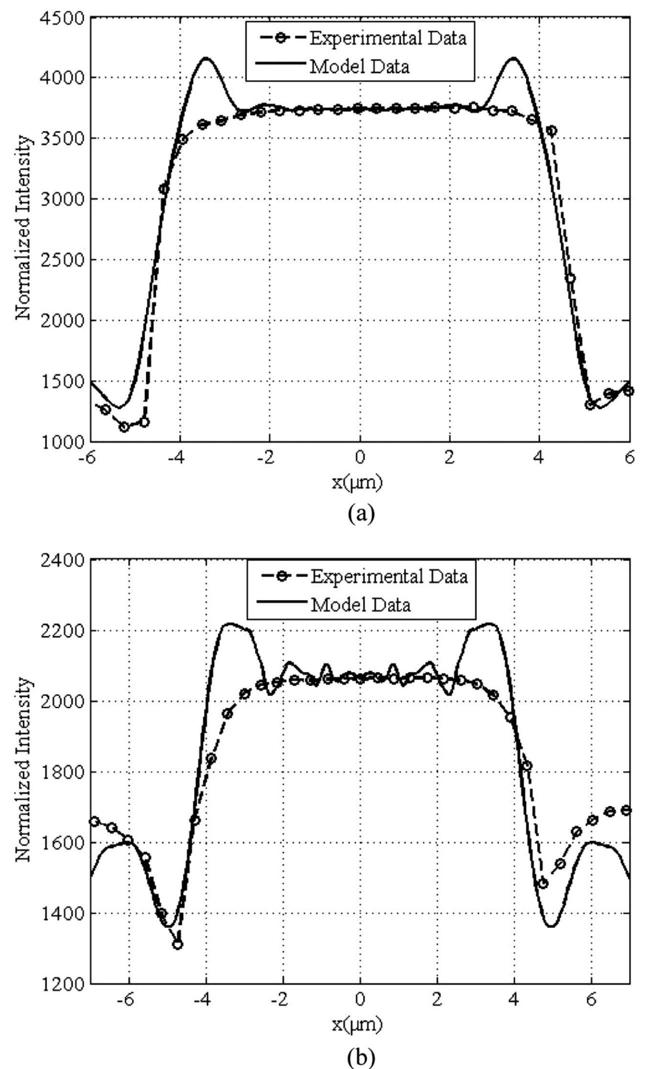

Fig. 5. Plot of experimental data and model for 10 μm wide gold interconnect for (a) $\lambda = 535$ nm at Section a-a of Fig. 1(c) and (b) $\lambda = 470$ nm at Section a-a of Fig. 1(c).

Figure 6(b) shows the comparison of model and experimental data at the narrow section for the wavelength of 470 nm. The overall reflectivity of gold at 470 and 530 nm is very different, around 0.4 to 0.6, and combined with the temperature dependence of the reflectivity, the diffraction patterns of both wavelengths along the gold line are different. By varying the optical distance z the same amount as was done for 530 nm, the model doesn't provide a good fit with the experimental data. Different values of z were tested, and the values listed in Table 2 give good qualitative fit for the data.

Table 2. Values of Fitting Parameters z, φ, Γ, γ

Wavelength (nm)	a (μm)	z (μm)	φ (rad)	Γ	γ
535	5	20	2.2	0.64	3700
	0.5	3.75	2.2	0.64	3400
470	5	15	2.12	0.9	2068
	0.5	5.75	2.12	0.9	1068

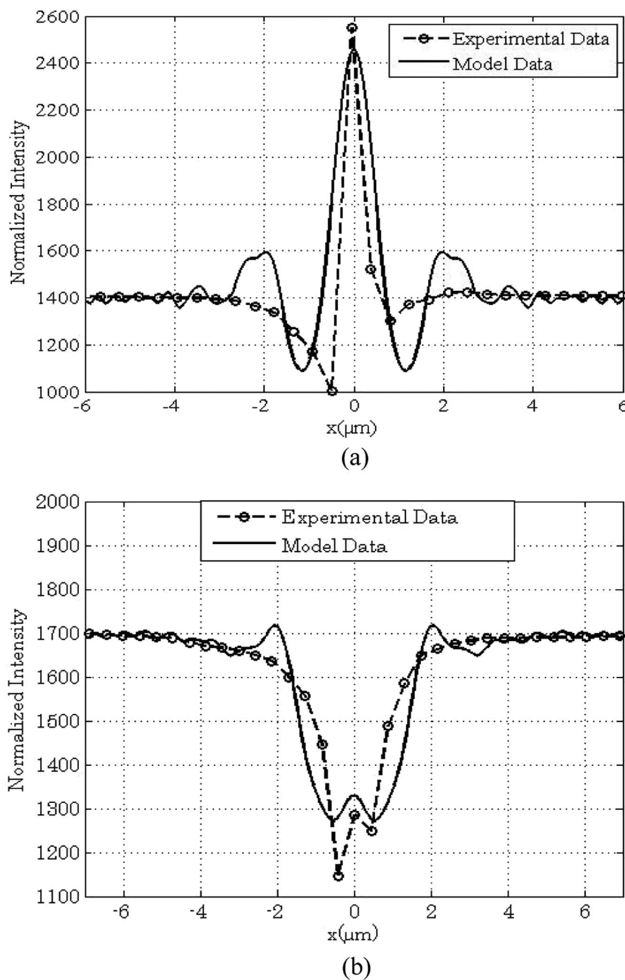

Fig. 6. Plot of experimental data and model for 1 μm wide gold interconnect for (a) $\lambda = 535$ nm at Section b-b of Fig. 1(c) and (b) $\lambda = 470$ nm at Section b-b of Fig. 1(c).

5. CONCLUSIONS

The use of thermoreflectance for temperature measurement has been well established based on its ability to generate a full field measurement, but there is an increasing desire to apply this technique to smaller spatial scales. As a result, there is a need to understand the impact of optical limits on the signal generated. This is the first known work applying a diffraction model to understand the thermoreflectance signal, and it will be useful in extending the technique to smaller scales. The diffraction model considers the reflection signal produced from samples of thin films on and from the substrate.

Four parameters are used in the model for fitting with experimental data. The results show good agreement between calculated and measured values. The overall reflectivity of gold at 470 and 530 nm changes significantly from 0.4 to 0.6, and this change is captured by the model. The diffraction patterns for 470 and 530 nm produce different data profiles. Furthermore, at each wavelength due to diffraction the thermoreflectance signal is significantly different for the narrow (1 μm wide) line as compared to the wider (10 μm line).

Dean's Graduate Engineering Fellowship (1); Packard Fellowship (1).

S. Kureshi was awarded a Dean's Graduate Engineering Fellowship and Packard Fellowship during the course of this work.

REFERENCES

1. International Technology Roadmap for Semiconductors, 2013, available at http://www.itrs.net/Links/2013ITRS/2013Chapters/2013Interconnect.pdf.
2. O. Nakabeppu and T. Suzuki, "Microscale temperature measurement by scanning thermal microscopy," J. Therm. Anal. Calorim. **69**, 727–737 (2002).
3. D. Cahill, K. Goodson, and A. Majumdar, "Thermometry and thermal transport in micro/nanoscale solid-state devices and structures," J. Heat Transfer **124**, 223–241 (2002).
4. J. Christofferson and A. Shakouri, "Thermoreflectance based thermal microscope," Rev. Sci. Instrum. **76**, 024903 (2005).
5. J. Christofferson, K. Maize, Y. Ezzahri, J. Shabani, X. Wang, and A. Shakouri, "Microscale and nanoscale thermal characterization techniques," in *Thermal Issues in Emerging Technologies*, Cairo, Egypt, 2007, pp. 3–9.
6. P. L. Komarov, M. G. Burzo, and P. E. Raad, "CCD thermoreflectance thermography system: methodology and experimental validation," in *12th International Workshop on Thermal Investigations of ICs and Systems (THERMINIC 12)*, Nice, France, 2006.
7. C. Cardenas, D. Fabris, S. Tokairin, F. Madriz, and C. Y. Yang, "Thermoreflectance measurement of temperature and thermal resistance of thin film gold," J. Heat Transfer **134**, 111401 (2012).
8. C. Cardenas, "Thermoreflectance temperature measurement and application to gold thin films and carbon nanofibers," M.S. thesis (Santa Clara University, 2011).
9. K. Yazawa, D. Kending, D. Hernandez, K. Maze, and A. Shakouri, "Challenges and opportunities for transient thermal imaging of microelectronic devices," in *18th International Workshop on Thermal Investigations of ICs and Systems (THERMINIC 18)*, September 2012, pp. 25–27.
10. A. Sommerfeld, *Optics, Volume IV of Lectures on Theoretical Physics* (Academic, 1954).
11. J. W. Goodman, *Introduction to Fourier Optics*, 3rd ed. (Roberts, 2005).
12. M. Born and E. Wolf, *Principles of Optics*, 7th ed. (Cambridge University, 1999).
13. F. L. Pedrotti, L. M. Pedrotti, and L. S. Pedrotti, *Introduction to Optics*, 3rd ed. (Addison-Wesley, 2006).
14. F. R. Madriz, J. R. Jameson, S. Krishnan, X. Sun, and C. Y. Yang, "Circuit modeling of high-frequency electrical conduction in carbon nanofibers," IEEE Trans. Electron. Dev. **56**, 1557–1561 (2009).
15. F. R. Madriz, J. R. Jameson, S. Krishnan, X. Sun, and C. Y. Yang, "Test structure to extract circuit model of nanostructures operating at high-frequencies," in *IEEE International Conference on Microelectronic Test Structures* (IEEE, 2009), pp. 36–38.
16. S. Tokairin, K. Read, P. Wilhite, J. Chen, D. Fabris, and C. Y. Yang, "Thermoreflectance of carbon nanofibers: Joule Heating experiment and calibration," in *10th International Conference on Heat Transfer, Fluid Mechanics and Thermodynamics*, Orlando, Florida, July 14–16, 2014.
17. A. Beran, "The reflectance behavior of gold at temperatures up to 500°C," Tschermaks Mineralogische und Petrographische Mitteilungen **34**, 211–215 (1985).
18. S. Grauby, A. Salhi, L. P. Lopez, W. Claeys, B. Charlot, and S. Dilhaire, "Comparison of thermoreflectance and scanning thermal microscopy for microelectronic device temperature variation imaging: calibration and resolution issues," Microelecton. Rel. **48**, 204–211 (2008).
19. S. J. Orfanidis, Electromagnetic Waves and Antennas, available online at www.ece.rutgers.edu/~orfanidi/ewa (2008).
20. E. Palik, *Handbook of Optical Constants of Solids* (Elsevier, 1998).